TSUNAMI HAZARD ASSESSMENT IN NORTHERN EGYPT USING NUMERICAL SIMULATION

Abutaleb Ali[*] **Supervisor: Bunichiro SHIBAZAKI**[**]
MEE16717 **Yushiro FUJII**[**]

ABSTRACT

To investigate the tsunami hazard along the northern coast of Egypt, we performed numerical simulations of tsunamis generated by tsunamigenic earthquakes in the Eastern Mediterranean region using TUNAMI-N2 (Tohoku University Numerical Analysis Model for investigation of Near field tsunamis) code. We considered a different resolution of gridded bathymetry data (GEBCO 1 arc-min and the latest updated version of 2014 30 arc-sec). We investigated a set of various scenarios (historical, credible and the worst near-field case). We presented the result of five scenario earthquakes with magnitude 7.8 to 8.6. We referred the earthquake fault parameters from two different previous studies. We assumed six virtual forecast points as output points along the Egyptian coast to calculate the tsunami waveforms. We investigated the worst case tsunami scenario toward the northern coast of Egypt, especially the Nile delta region to examine the tsunami travel time and maximum tsunami height. The results indicated that the first tsunami wave arrived at the Egyptian coastline about one hour after the occurrence of the earthquake. The maximum tsunami heights for the worst case scenario (Mw 8.6) of the 142 earthquake were about 5.7 m and 4.8 m at Alexandria city using the 30 arc-second and 1 arc-minute bathymetry data, respectively.

Keywords: Tsunami hazard, Numerical simulation, Tsunamigenic earthquake, Eastern Mediterranean, Maximum tsunami height.

1. INTRODUCTION

The Egyptian Mediterranean coastal zone is one of the tsunami prone areas in northern Africa and affected by very strong tsunamigenic earthquakes in the past, for instance the most severe events occurred on 21st of July, 365 AD, and 8th of August, 1303 AD earthquakes. These tsunami events caused widespread damage and destroyed the Nile Delta region, northern part of Egypt. The historical record indicates that the risk of tsunamis in Egyptian coastal zones is extremely high due to its highly dense population. As well, most of the tsunamis take place near the shore, therefore there is a very little time to hit the whole area. Moreover, in 2015 agreements were signed by Egypt and Russia to construct the first Egypt's nuclear power plant to boost electricity at El-Dabaa area, which is located on the Egyptian Mediterranean coast, 160 km west of Alexandria city. Therefore, it is necessary to study the probable tsunami hazard by analyzing potential worst-case tsunami scenarios around the eastern Mediterranean region and evaluate their impacts on the Egyptian coastal zones especially on Nile Delta region, Alexandria, the largest Egyptian coastal city to raise awareness and contribute to disaster risk reduction.

[*]National Research Institute of Astronomy and Geophysics (NRIAG), Seismology department, Egyptian National Seismic Network (ENSN), Helwan, Egypt.
[**]International Institute of Seismology and Earthquake Engineering (IISEE), Building Research Institute (BRI), Tsukuba, Japan.

2. METHODOLOGY AND THEORY

2.1. Ocean bottom deformation

Tsunami waves are generated in the sea mostly due to vertical displacements of the ocean floor by earthquake faulting. This deformation is considered as the initial condition for a tsunami source. Therefore, the fault parameters are necessary to estimate the displacement of sea floor deformation using the Okada's formula (1985).

2.2. Governing Equations in Cartesian and Spherical Coordinate Systems

For the Cartesian coordinate system, the continuity and momentum equations are as follows: (Imamura et al., 2006).

$$\frac{\partial \eta}{\partial t} + \frac{\partial M}{\partial x} + \frac{\partial N}{\partial y} = 0 \tag{1}$$

$$\frac{\partial M}{\partial t} + \frac{\partial}{\partial x}\left(\frac{M^2}{D}\right) + \frac{\partial}{\partial y}\left(\frac{MN}{D}\right) + gD\frac{\partial \eta}{\partial x} + \frac{gn^2}{D^{7/3}}M\sqrt{M^2+N^2} = 0 \tag{2}$$

$$\frac{\partial N}{\partial t} + \frac{\partial}{\partial y}\left(\frac{N^2}{D}\right) + \frac{\partial}{\partial x}\left(\frac{MN}{D}\right) + gD\frac{\partial \eta}{\partial y} + \frac{gn^2}{D^{7/3}}N\sqrt{M^2+N^2} = 0 \tag{3}$$

where, η is water level, M and N are discharge flux in x and y directions respectively, h is the water depth, t is the time , g is the gravitational acceleration, n is the manning roughness coefficient and D is the total depth (η + h).

For the Spherical coordinate system, the nonlinear shallow water equations considering bottom friction are as follows:

$$\frac{\partial \eta}{\partial t} + \frac{1}{Rcos\theta}\left[\frac{\partial M}{\partial \lambda} + \frac{\partial}{\partial \theta}(Ncos\theta)\right] = 0 \tag{4}$$

$$\frac{\partial M}{\partial t} + \frac{gD}{Rcos\theta}\frac{\partial \eta}{\partial \lambda} + \frac{1}{Rcos\theta}\frac{\partial}{\partial \lambda}\left(\frac{M^2}{D}\right) + \frac{1}{Rcos\theta}\frac{\partial}{\partial \theta}\left(cos\theta\frac{MN}{D}\right) + \frac{gn^2}{D^{7/3}}M\sqrt{M^2+N^2} = 0 \tag{5}$$

$$\frac{\partial N}{\partial t} + \frac{gD}{Rcos\theta}\frac{\partial \eta}{\partial \theta}(cos\theta\eta) + \frac{1}{Rcos\theta}\frac{\partial}{\partial \theta}\left(cos\theta\frac{N^2}{D}\right) + \frac{1}{Rcos\theta}\frac{\partial}{\partial \lambda}\left(\frac{MN}{D}\right) + \frac{gn^2}{D^{7/3}}N\sqrt{M^2+N^2} = 0 \tag{6}$$

where, λ is the latitude direction, M is the discharge flux in latitude direction, θ is the longitude direction, N is the discharge flux in longitude direction and R is the radius of the earth.

2.3. Stability conditions

Besides the uncertainty of the initial conditions and topography, the numerical instability in the computation is inevitable. Thus, to avoid this kind of errors, the Courant Fredric Lewy (CFL) condition $\Delta t \leq \Delta x/\sqrt{2gh_{max}}$ should be satisfied (Imamura et al., 2006), where, Δx and Δt are the spatial and temporal grid size respectively, hmax is the maximum still water depth and g is the gravitational acceleration. In this study, the temporal grid size (Δt) is set to be 2.0 s.

3. DATA

3.1. Bathymetry data

For simulation of tsunami propagation, we used bathymetry data downloaded from (General Bathymetric Chart of the Ocean GEBCO) website (http://www.gebco.net), with different resolution of a grid size of 1 arc-min and 30 arc-sec (Figure 1).

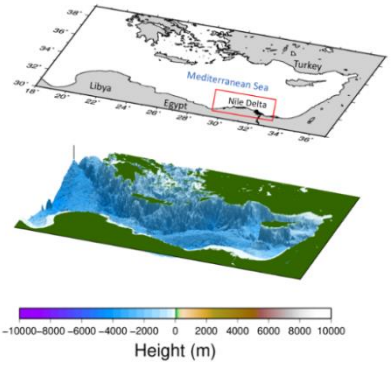

Figure 1. Digital bathymetry data for computational area.

3.2. Virtual coastal points

We assumed six output points along the north coast of Egypt as follows; EL-Salloum, Matrouh, Alexandria, Damietta, Portsaid and El-Arish from west to east. Then we investigate the calculated tsunami arrival times and tsunami wave heights at each reference location to reveal the tsunami threat. Figure 2 shows the location of the selected output points.

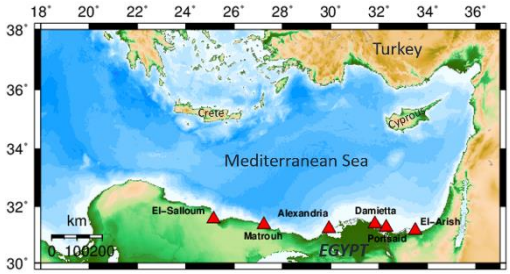

Figure 2. Distribution of assumed tide gauge stations along the Egyptian coast.

4. TSUNAMI SOURCE MODELS

We modeled all possible sources that would occur in the eastern Mediterranean region. Then we selected five scenarios which were considered as the most adverse scenarios (Figure 3) across the Egyptian coast to perform our analysis. Finally, we extracted the worst case scenario toward the Nile delta region; Alexandria city. The most obvious candidate scenario to be the worst case in the current work is the AD 142 event located in the eastern side of the Hellenic subduction zone to generate the potential maximum tsunami height along the Nile Delta region. The source parameters used in our analysis are derived directly from the published studies by Valle et al. (2014) and Mitsoudis et al. (2012) (Table 1).

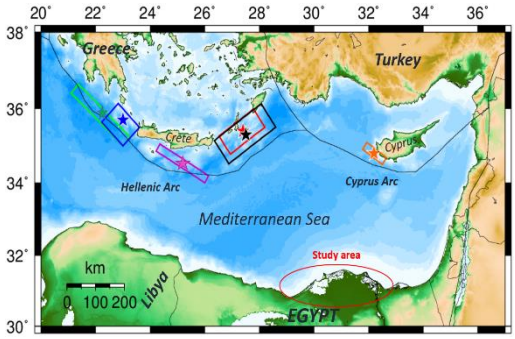

Figure 3. Source models for five worst scenarios toward the Egyptian coast.

Table 1. Earthquake fault parametrs for the worst-case scenario for the AD 142 event (Valle et al., 2014; Mitsoudis et al., 2012).

Scenario	Mw	Fault location		Length	Width	Strike	Dip	Rake	Slip	Top depth
		Lon (°E)	lat (°N)	km	km	deg	deg	deg	m	km
ST1	8.6	28.6	35.5	190	90	235	20	90	10	7.5
ST2	8.4	28.6	35.5	190	90	235	20	90	5	7.5

5. RESULTS AND DISCUSSION

5.1. Sea floor deformation

Figures 4 and 5 show the amount of uplift and subsidence due to earthquakes for the worst-case scenarios ST1 and ST2, where the red colors correspond to values of uplift and blue colors show the values of subsidence. In the case of ST1 with Mw8.6, the uplift value was 4.73 m while the subsidence value was 1.38 m but for the ST2 with Mw8.4, the uplift and subsidence values of 2.36 m and 0.69 m were calculated.

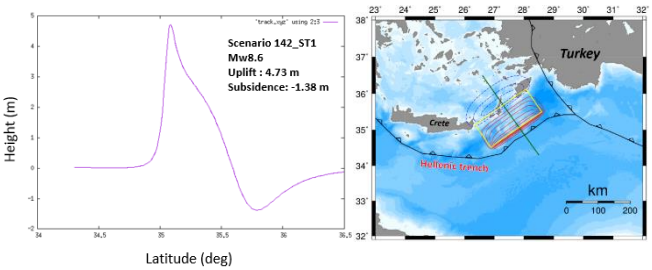

Figure 4. Computed sea floor deformation of the worst-case scenario earthquake ST1. The contour interval of uplift and subsidence are 0.7 m and 0.4 m, respectively.

5.2. Tsunami wave propagation

Figure 6 presents the snapshots of tsunami wave propagations for the worst-case scenario from the 142 AD event at initial condition (time zero), 10, 30, and 60 min after tsunami generation using 30 arc-sec bathymetry data. The snapshot at time zero demonstrates the tsunami generation i.e. water surface displacement caused by the ocean bottom deformation. From our computation, it is obvious that the main trend of the tsunami wave propagation was in the direction of the southeastern side. Through these analyses, we obtained the characteristics of tsunami wave behavior such as tsunami travel time and tsunami maximum height.

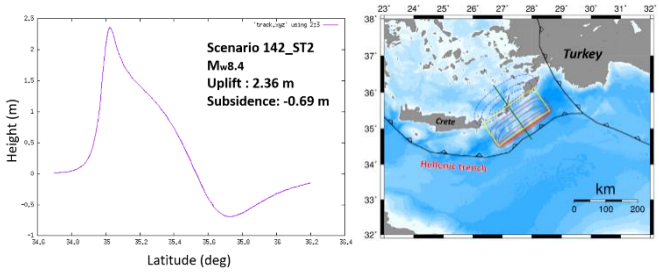

Figure 5. Same as Figure 4 but for the worst-case scenario earthquake ST2. The contour interval of uplift and subsidence are 0.4 m and 0.2 m, respectively.

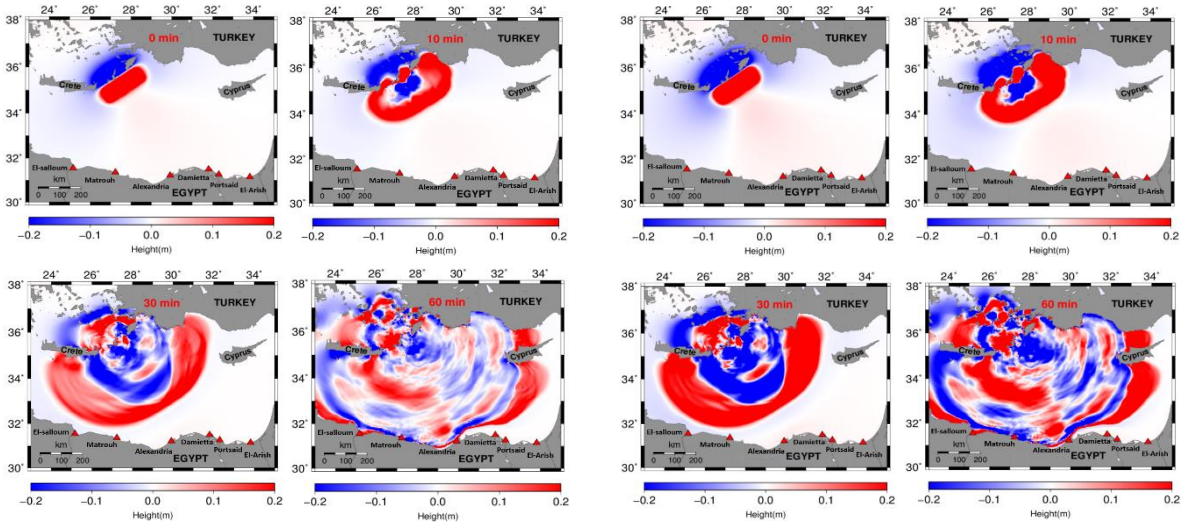

Figure 6. Snapshots of tsunami wave propagation from source area for the worst-case scenario ST1 (right) and ST2(left) using the 30 arc-sec bathymetry data.

5.2.1. Synthetic tsunami waveform

Figure 7 shows the comparison between synthetic tsunami waveforms for worst-case scenarios (ST1 and ST2) of the 142 AD earthquake using a different data sets 1 arc-min and 30 arc-sec. It seems that there is an agreement in tsunami arrival time between the results from different bathymetry data for both cases at each coastal point while the tsunami heights are slightly different. On the other hand, at the initial time, the positive tsunami amplitudes were observed at all the assumed forecast points. The virtual tide gauge station located at Alexandria city had a significant amplitude for both cases while the smaller amplitude was recorded at Portsaid and El Salloum stations.

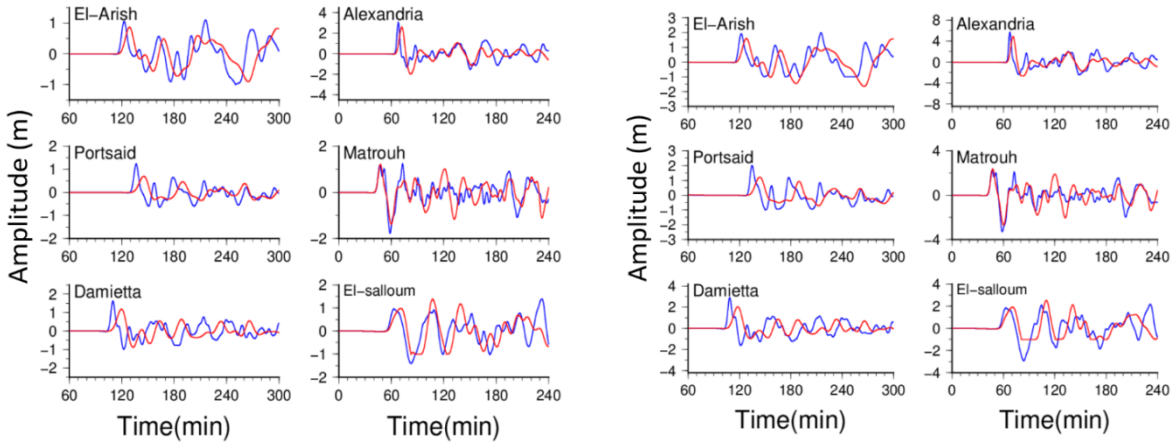

Figure 7. Comparison of the calculated tsunami waveforms for the worst-case tsunami scenario 142 AD earthquake ST1 (right) and ST2 (left) using GEBCO 1 arc-min (red lines) and GEBCO_2014 30 arc-sec (blue lines) bathymetry data.

5.2.2. Maximum tsunami height

Figure 8 compares calculated maximum tsunami heights at different output points for both cases using the 1 arc-min and 30 arc-sec bathymetry data. The highest tsunami was recorded at the Alexandria station, around 5.8 m for ST1 with Mw8.6 using GEBCO 30 arc-sec bathymetry data but 4.8 m using GEBCO 1 arc-min. Moreover, the tsunami height of more than 2 m was calculated at Damietta, Matrouh and El salloum cities.

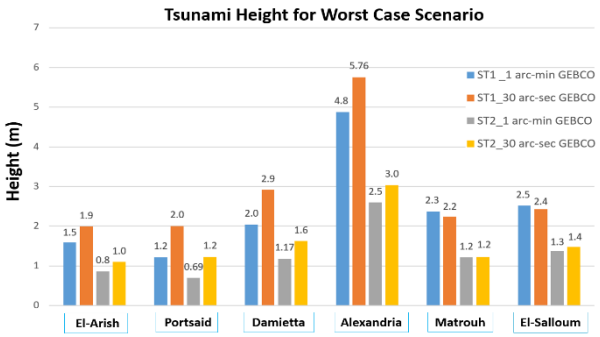

Figure 8. Summary of computed maximum tsunami height for worst-case scenarios using different data sets.

5.2.3. Tsunami travel time

Figure 9 shows the travel time of initial tsunami wave (TTIT) at output points for the worst-case scenario ST1 and ST2 using GEBCO 1 arc-min and GEBCO 30 arc-sec bathymetry data. It is an important factor in tsunami hazard assessment to identify the time required for the first tsunami wave to travel from the source to a given point on coastlines.

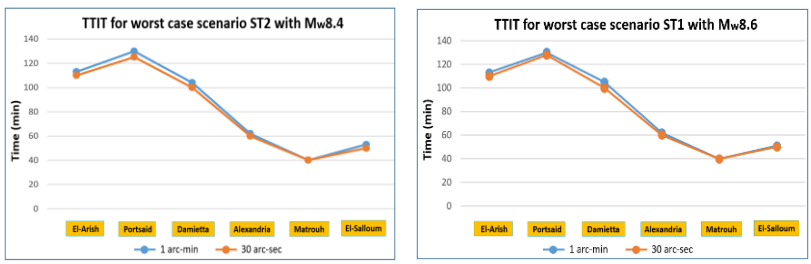

Figure 9. Travel time of initial tsunami wave (TTIT) at virtual coastal points for the worst-case scenario ST1 (right) and ST2 (left) using different data sets.

6. CONCLUSIONS

We evaluated the tsunami hazard for the Egyptian Mediterranean coastline (north coast of Egypt) by performing numerical computation of tsunami propagation using TUNAMI-N2 code developed by Disaster Control Research Center, Tohoku University. The numerical model based on the shallow water approximation was solved with staggered leap-frog scheme using a finite difference method. We considered scenarios of historical earthquakes and selected the worst-case scenario of the earthquake with Mw8.6.

Two different kinds of resolution of digital bathymetry data were used to conduct the simulation; GEBCO 1 arc-minute and latest version GEBCO 30 arc-seconds bathymetry data. The latter finer bathymetry data gives more accurate results at narrow seas or inner bays. However, in the case of the open ocean, the difference is not so large.

From numerical simulation the tsunami travel time and maximum tsunami height were extracted at the six virtual forecasting points. The Matrouh coastal point recorded the first arrival of tsunami wave of about 40 minutes. The Portsaid coastal point recorded the latest arrival time of about 130 min.

The numerical results indicate that the most vulnerable area to face the tsunami hazards is the Nile Delta region, especially Alexandria city. The maximum tsunami height is about 5 m one hour after the origin time. Therefore, special attention must be taken for this region in order to increase the awareness for reducing the vulnerability.

Our results would be useful for public authorities and decision-makers in creating a database on tsunami scenarios for the eastern Mediterranean region to identify risk in each scenario at coastal areas in order to develop appropriate countermeasures and preparedness to cope with the future tsunami hazard.

ACKNOWLEDGEMENTS

I would like to express my gratitude to my supervisors Bunichiro SHIBAZAKI and Yushiro FUJII for their continuous support of my MSc study and linked research, for their guidance, insightful comments, suggestions, instructions and the hard questions which incented me to develop my thesis from various perspective during this study. Also, I would like to extend my deep thanks to all staff members of IISEE, BRI and National Graduate Institute for Policy Studies (GRIPS) for their support, cooperation, and elaboration of whole course materials.

REFERENCES

Imamura F., Yalcinar A.C., Ozyurt G., 2006, DCRC, Tohoku University, Japan.

Mitsoudis, D. A., Flouri, E. T., Chrysoulakis, N., Kamarianakis, Y., Okal, E. A., & Synolakis, C. E., 2012., Coastal Engineering, 60, 136-148.

Okada, Y., 1985. Bulletin of the seismological society of America, 75(4), 1135-1154.

Valle, B. L., Kalligeris, N., Findikakis, A. N., Okal, E. A., Melilla, L., & Synolakis, C. E., 2014. Proceedings of the Institution of Civil Engineers-Engineering and Computational Mechanics, 167(3), 99-105.

Websites: General Bathymetric Chart of the Oceans (GEBCO), https://www.gebco.net/.